Structure
Article

Structural Dynamics of the Magnesium-Bound Conformation of CorA in a Lipid Bilayer

Olivier Dalmas,[1] Luis G. Cuello,[1,2] Vishwanath Jogini,[1,3] D. Marien Cortes,[1,2] Benoit Roux,[1] and Eduardo Perozo[1,*]
[1]Department of Biochemistry and Molecular Biology, Institute for Biophysical Dynamics, The University of Chicago, IL 60637, USA
[2]Present address: Department of Cell Physiology and Molecular Biophysics, Center for Membrane Protein Research, Texas Tech University Health Science Center, Lubbock, TX 79430, USA
[3]Present address: D.E. Shaw Research, Hyderabad, India
*Correspondence: eperozo@uchicago.edu
DOI 10.1016/j.str.2010.04.009

SUMMARY

The transmembrane conformation of *Thermotoga maritima* CorA, a magnesium transport system, has been studied in its Mg^{2+}-bound form by site-directed spin labeling and electron paramagnetic resonance spectroscopy. Probe mobility together with accessibility data were used to evaluate the overall dynamics and relative arrangement of individual transmembrane segments TM1 and TM2. TM1 extends toward the cytoplasmic side creating a water-filled cavity, while TM2 is located in the periphery of the oligomer, contacting the lipid bilayer. A structural model for the conserved extracellular loop was generated based on EPR data and MD simulations, in which residue E316 is located toward the five-fold symmetry axis in position to electrostatically influence divalent ion translocation. Electrostatic analysis of our model suggest that, in agreement with the crystal structure, Mg^{2+} -bound CorA is in a closed conformation. The present results suggest that long-range structural rearrangements are necessary to allow Mg^{2+} translocation.

INTRODUCTION

Magnesium, the most abundant divalent cation in cells, plays essential roles in a variety of key biological processes, being an ubiquitous cofactor in a myriad of enzymatic reactions while also contributing to genomic stability. Controlling Mg^{2+} concentrations within a tight range is therefore critically important in cellular homeostasis. In prokaryotes, magnesium uptake is mainly mediated by the CorA family of membrane proteins, so far the most exhaustively studied Mg^{2+} transport system (Hmiel et al., 1986, 1989; Kehres et al., 1998; Maguire, 1992). The recently determined divalent-bound CorA structure (Eshaghi et al., 2006; Lunin et al., 2006; Payandeh and Pai, 2006) revealed a homopentamer with a large, funnel-like intracellular domain linked to two transmembrane helices (TM1 and TM2) by a long stalk helix (Lunin et al., 2006). The structure is also characterized by a long (~40 Å), narrow hydrophobic pore that lacks any obvious coordinated Mg^{2+} ions. Two divalent ion binding sites flank both ends of this long and narrow pore: In the base of the funnel, a Mg^{2+} ion is stabilized by Aspartate D277 at the interface between two adjacent subunits (Eshaghi et al., 2006). Whereas in high [Ca^{2+}], an observed density around G309, close to the extracellular site, appears to represent a bound hydrated divalent ion (Payandeh and Pai, 2006).

The large cytoplasmic domain has been proposed to act as a regulatory domain that controls the transport cycle (Lunin et al., 2006). Two divalent cation binding sites located away from the putative permeation pathway have been suggested as a possible divalent cation sensor (DCS). The first divalent binding site, seen in all three structures, is coordinated by the carboxylic groups from D89 and D253 (Lunin et al., 2006). A second binding site has only been seen in the higher resolution structures (Eshaghi et al., 2006; Payandeh and Pai, 2006) and appears to be coordinated by the carboxylic groups from E88, D175, and D253. These sites are thought to serve as the trigger that initiates the conformational wave responsible for Mg^{2+} translocation.

The periplasmic loop connecting TM1 to TM2 contains the highly conserved motif "GMN" and "MPEL" common to most members of the CorA family. However, this region is disordered in all of the available crystal structures. Given the extracellular exposure of this loop, it has been suggested as a potential initial magnesium binding site and the first stage during the process of translocation across the membrane (Lunin et al., 2006). Mutations in this region have a strong impact on transport activity in the yeast's CorA ortholog (Schindl et al., 2007; Weghuber et al., 2006), while a recent NMR study suggests it might play a role in divalent cation recognition (Hu et al., 2009). Nevertheless, in vivo survival assays have recently been used to argue against an essential role of the extracellular loop in Mg^{2+} uptake (Payandeh et al., 2008). These apparently contradictory results, together with a low sequence conservation among family members have been used to question whether *Tm*CorA behaves as a bona fide ligand-gated ion channel (Dalmas, 2007).

Here, we used site-directed spin labeling and EPR spectroscopy to study the structural dynamics of the nonconductive Mg^{2+}-bound form of CorA from Thermotoga maritima (*Tm*CorA), reconstituted in a lipid bilayer. Our data demonstrate that the membrane architecture of *Tm*CorA largely corresponds to the three-dimensional crystal structure and shows that the transmembrane segments are the most dynamic region of the molecule. Furthermore, a structural model of the highly conserved periplamsic loop was developed and refined based on EPR solvent accessibility and interspin label proximity

 ©2010 Elsevier Ltd All rights reserved

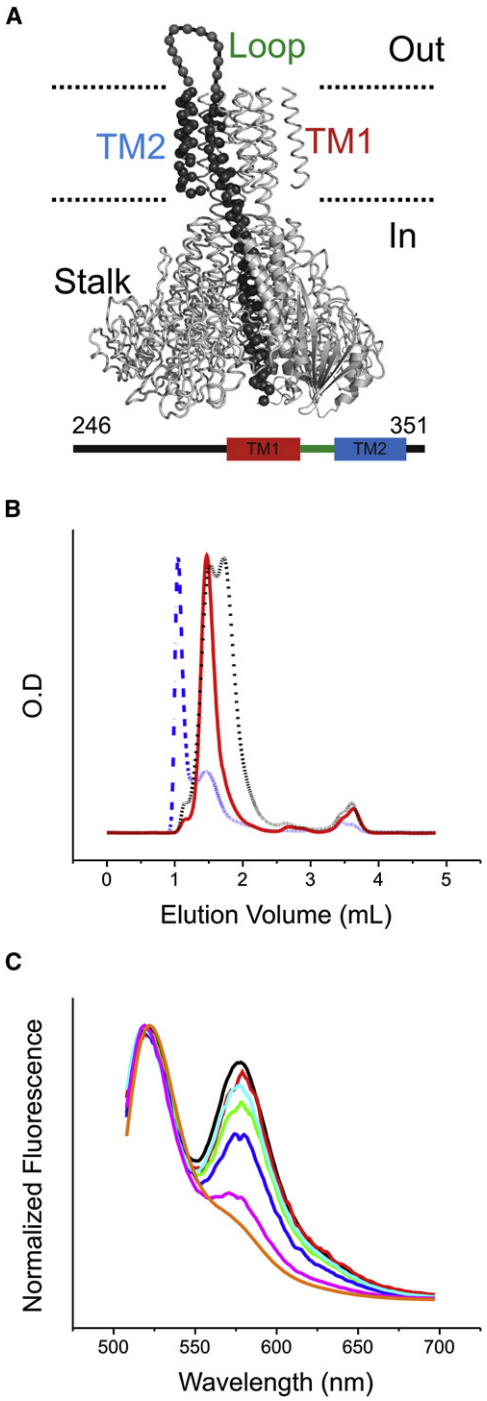

Figure 1. Biochemical Preparation of Single Cysteine Mutants and Optimized Reconstitution

(A) Cysteine scan mutagenesis of *Tm*CorA covers four segments: the stalk helix, TM1, the periplasmic loop, and TM2. Individual mutation sites are depicted by black spheres at the Cα.

(B) CorA hydrodynamic profile as assayed by FPLC showing representative gel filtration chromatograms of a typical monodisperse peak for WT or well folded and stable mutants (red trace), an aggregated mutant (blue trace), and an unstable mutant (black). Only mutants with a monodisperse profile were further processed for spectroscopic measurements.

(C) FRET assay monitors protein-protein aggregation induced by the lipid composition of the membrane: asolectin (black), POPE-POPG 3:1 (red), *E. coli* polar lipids (green), egg extract (dark blue), POPC-POPG 3:1 keep at room temperature or 4°C (purple) or frozen and thawed (cyan), DDM micelles solution (orange).

measurements. Our model points to the possible role of the loop in extracellular Mg^{2+} recognition and permeation as suggested by the shape and magnitude of the calculated electrostatic potential map at the entry of the permeation pathway.

RESULTS

The Conformation of Membrane-Embedded CorA from EPR Spectroscopy Analysis

To evaluate the architecture of *Tm*CorA embedded in a membrane bilayer, we carried out cysteine scanning mutagenesis covering both transmembrane segments and the entire length of the stalk helix, using a cysteine-free background (C135S) (Figure 1A). Overall, cysteine mutations did not alter the protein folding nor the hydrodynamic behavior of the protein as evaluated by analytical gel filtration chromatography (Figure 1B) and corresponds to the molecular weight of a pentamer as determined by MALS-UV-RI (see Figure S1 available online). Of the full complement of 112 cysteine mutations, only five failed to express (positions 250, 271, 291, 320, and 348) and four others showed some protein folding/stability issues (positions 251, 294, 304, and 319), none of which were included in this study. This represents less than 9% of the total number of mutants. Additional insights on the perturbation effects of the mutagenesis on CorA were obtained by following the normalized expression level of each mutant (Figure S2). Except for those that did not express or were folding-compromised, most healthy mutants can reach expression levels between 10 and 15 mg/l. Although we cannot fully rule out the possibility of local perturbation introduced by the spin probe, our monitoring of the hydrodynamic behavior of the spin-labeled mutants strongly suggests that the overall folding and assembly in the vast majority of the CorA mutants was not altered. Our previous work, as well as the data set presented here, indicates that spin label induced local unfolding effects are very uncommon and when they appear can be easily identified as they would appear as mobility outliers in an extensive cystein scan (Perozo et al., 1998, 1999). In all evaluated mutants, the labeled protein remained monodisperse once reconstituted at a 1/1500 protein/lipid ratio (mol/mol) in a mixture of POPC:POPG (3:1) (Figure 1C).

Solvent accessibility was evaluated from power saturation experiments using fast relaxing agents soluble either in water or lipid (NiEdda and O_2, respectively) (Altenbach et al., 1989; Farahbakhsh et al., 1992). The mobility of the spin probe attached at different position of the protein was measured from the inverse of the width of the central resonance line (ΔH^{-1}) as previously described (McHaourab et al., 1996). Figure 2 shows the environmental parameter profile for the present CorA mutant set measured in presence of 10 mM Mg^{2+}. These conditions stabilize a nontransporting/nonconducting form of CorA. The O_2 accessibility profile clearly demonstrates the presence of two transmembrane (TM) segments, with TM2 showing higher overall O_2 accessibility than TM1, an indication that TM2 is in direct contact with the lipid bilayer. Indeed, the magnitude and

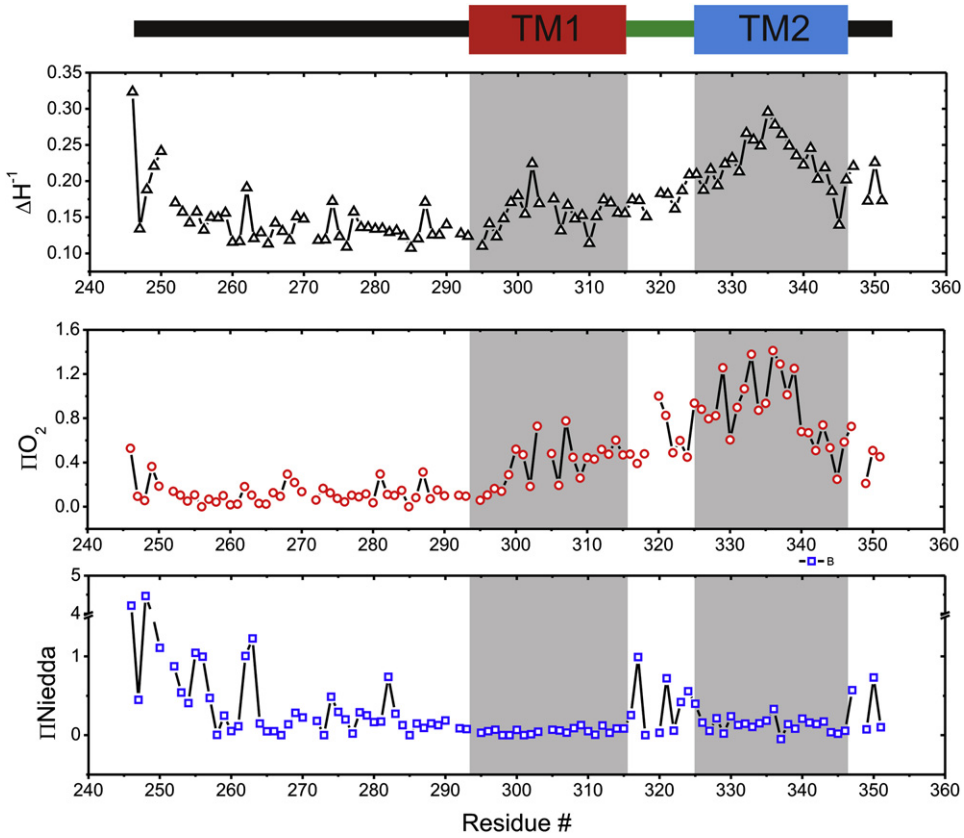

Figure 2. Residue-Specific Environmental Parameter Profiles Obtained along the Cystein Scan

Mobility parameter ΔH_0^{-1} (top, black triangles), oxygen accessibility parameter ΠO_2 (middle, red circles), and NiEdda accessibility parameter ΠNiEdda (bottom, blue squares). Grayed areas represent the membrane assignment derived from CorA EPR data.

periodicity of ΠO_2 along TM2 suggest an ordered but highly dynamic helical backbone buried in the membrane, consistent with its low NiEdda accessibility. Its overall high probe mobility also correlates well with the high temperature factors observed for this region in the crystal structure. The NiEdda accessibility data, on the other hand, argue strongly for a water-filled cavity on the cytoplasmic side that tapers off shortly after residue 283 in the middle of the cavity. The characteristic environments of each of the structural element in the CorA monomer are best summarized by Box plots of EPR parameters (Figure S4), where the high dynamic behavior of TM2 is evident even in comparison with highly mobile regions as in the extracellular loop.

To correlate structural properties of CorA in a lipid bilayer with its detergent-stabilized crystal structure, the EPR environmental parameters were mapped and color coded on the Mg^{2+}-bound structure (Figures 3A–3C). The probe mobility reports a complex and rather restrictive environment on the cytoplasmic entrance of the funnel with a gradual reduction in local dynamics as the pore narrows. This is consistent with the reduction in ΠNiEdda as the water-filled cavity in the stalk leads to the constricted transmembrane pore. On the cytoplasmic side, the mapping of ΠNiEdda agrees well with a water-filled cavity, where residues with high ΠNiEdda value face the center of the cavity. This feature is highlighted by superimposing ΠNiEdda values on a helical wheel polar representation (Figure 3D). Finally, ΠO_2 values mapped on the structure highlight the face of the TM2 helix in direct contact with the lipid bilayer.

As expected for a spin-labeled symmetric homo-oligomer (Altenbach et al., 1989; Perozo et al., 2002), evidence of inter-subunit proximity due to spin-spin coupling was found in at least 10 positions that line most of the permeation pathway. When mapped on the Mg^{2+} CorA structure, these are located mostly facing the funnel cavity and at the ends of the narrow transmembrane pore (Figure 4). However, it is important to note that while all of the pore lining residues display a characteristic set of EPR spectra, the majority of these positions show no evidence of spin-spin dipolar interactions. This is likely a consequence of poor labeling efficiency due to steric hindrance in these narrow cavities.

NiEdda and O_2 Accessibility Determine the Position of CorA within the Bilayer

Molecular oxygen is known to partition in a lipid bilayer with an increasing concentration gradient toward the hydrophobic core of the membrane. The shape of the gradient follows an oscillating parabolic function where the maximum roughly correspond to the center of the lipid bilayer (Altenbach et al., 1994). Therefore, the O_2 footprint of the lipid bilayer can be used to determine the position of TM2 relative to the center of the bilayer (Figure 5). A maximum at residue 335 in TM2, together with the boundaries

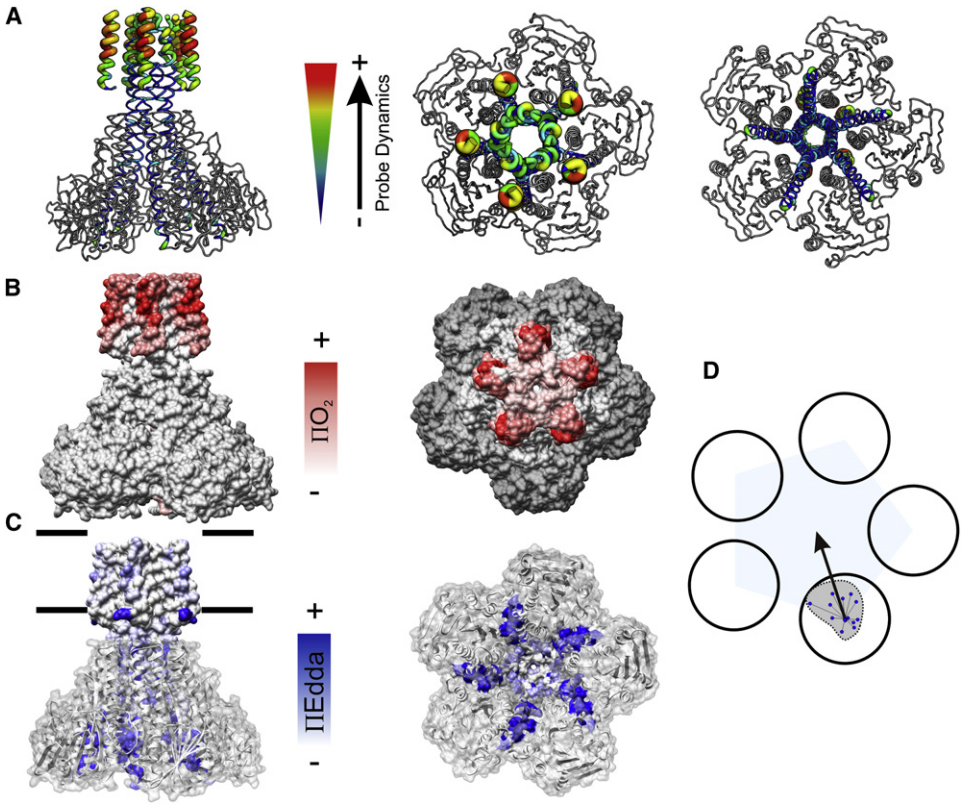

Figure 3. Overall Agreement between X-ray Structure and Experimental EPR Data and Positioning of the Membrane Bilayer

(A) Probe mobility parameter ΔHo^{-1} mapped onto the CorA structure both color coded and "sausage" scaled for visual clarity. The structure is shown in its side (left) periplasmic (center) and cytoplasmic (right) representations.

(B) O_2 accessibility EPR data exhibit a clear surface on TM2 that is exposed to lipid shown in its side (left) and periplasmic (right) views.

(C) NiEdda accessibility data were mapped and color coded from white to dark blue and shown in its side (left) and cytoplasmic (right) views (see also Figure S5).

(D) Polar representation of normalized NiEdda collision frequency from residue 247 to 265. The helix is represented as a wheel, seen from the top and was oriented accordingly to the structure. The resultant vector is represented by a black arrow and predicts the orientation of the helix regarding the center of the cavity.

delimited by ΠNiEdda, suggest that the likely footprint of the lipid bilayer in CorA is between residues W325 and F345 (a region not fully resolved in the X-ray structure). This observation is well in line with the propensity of aromatic residues to play the role of membrane anchor in most membrane proteins (Killian and von Heijne, 2000).

Regarding TM1, while its extracellular membrane "exit" point is clearly identifiable from the ΠNiEdda profile around residue N314 (Figure 2), its cytoplasmic boundary was not as well defined. This is a reflection of the position of TM1 near the five-fold symmetry axis as a continuation to the long cytoplasmic helix anchoring the funnel. Given the size of ΠNiEdda (cross section of around 5–7 Å), it is unlikely to access the narrow sections of the pore. Indeed, because of its volume ΠNiEdda accessibility often underestimates actual water exposure near sterically hindered volumes.

Modeling of the Conserved Periplasmic Loop

Generally, proteins exploit the conformational variability of loop regions to carry out different biological functions such as substrate recognition or signal transduction (Gouaux and Mackinnon, 2005). The CorA family is defined by the presence of two signature sequences: "GMN" at the end of TM1 and "MPEL" located in the short periplasmic loop region. Even at its highest resolution (2.9 Å) (Eshaghi et al., 2006), the weakness of the CorA structures extracellular loop electron density has precluded the construction of an explicit structural model of this segment. Other available CorA structures show no discernible density for residues Phe315 to Gly326 (Lunin et al., 2006; Payandeh and Pai, 2006).

We have taken advantage of the present spectroscopic data set to evaluate the conformation of this functionally important region. Recently, our lab has developed the "Pseudoatom-Driven Solvent Accessibility Refinement" (PaDSAR) method to refine membrane protein structures by restrained molecular dynamic simulation using parameterized solvent accessibility data from EPR experiments (Sompornpisut et al., 2008). This method was initially validated by refolding distorted conformations of KcsA (from 2 to 30 Å RMSD) and was able to converge toward the native structure within a 1–3 Å backbone RMSD (Sompornpisut et al., 2008). The method has also been proven useful to model the N-terminal domain of a mechanosensitive channel not resolved in the X-ray crystal structure (Vasquez et al., 2008). Here, we combined PaDSAR with the Rosetta loop building (Bonneau et al., 2002; Rohl et al., 2004; Schueler-Furman et al., 2005), as illustrated in Figure 6, to generate an

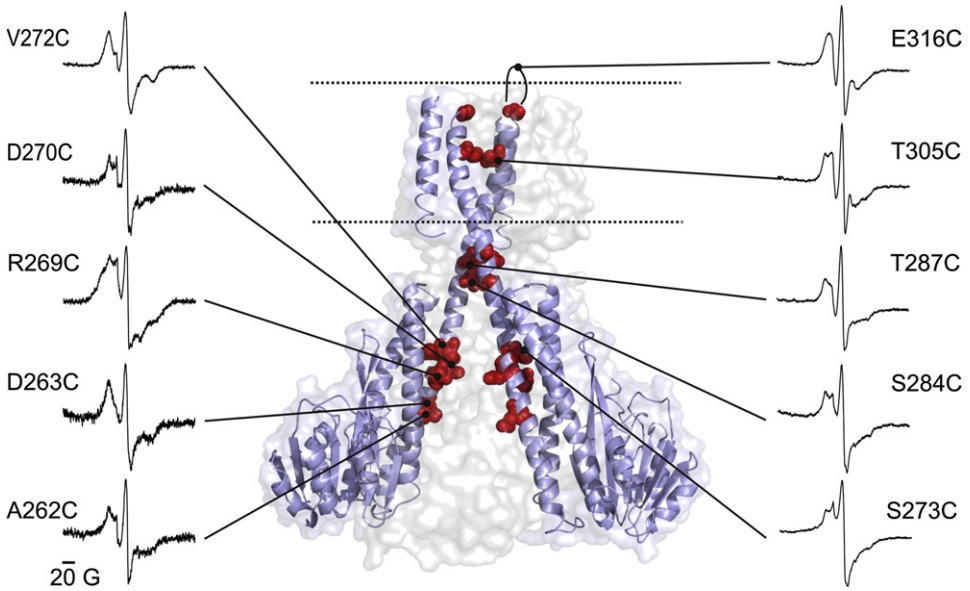

Figure 4. Close Proximity of the Spin Probe along the Permeation Pathway
Positions where spin-spin interactions were detected are highlighted by red CPK representations of the original side chains along the structure of CorA. In each case, the amplitude normalized fully labeled CW-EPR spectra is shown as indicated by the connecting lines. Only two monomers are shown for clarity.

explicit loop structure based on our EPR accessibility data. The loop obtained using Rosetta was connected to TM1 and TM2 on one protomer and was symmetrized 5-fold. Steric clashes were manually avoided and the regularized structure by energy minimization seeded as a starting conformation for the EPR-constrain refinement. The start and end points of the PaDSAR simulation are superimposed on Figure 6 (bottom), which together with intermediate structures derived from simulation trajectory point to a relatively narrow convergence of the final model with a backbone RMSD around 1.3Å (Figure S7). The agreement of our model with experimental data was evaluated by regression analysis of calculated versus measured accessibility before and after imposing the EPR constrains. The correlation coefficient R^2 increases from 0.2 to 0.73 and shows a much better agreement of the experimental values by the refined model (Figure 7A, right). This is also confirmed from mapping the NiEdda accessibility data onto the converged model, as shown in Figure S8.

The most important observation from our model is that Glutamate 316 has moved considerably toward the center of the axis of symmetry (Figure 7B). This residue displays the strongest spin-spin coupling in CorA (see Figure 4) and in our final model seems to adopt a position that could accommodate a positive ion the size of a hydrated Mg^{2+}.

The Magnesium-Bound Conformation of *Tm*CorA Is Sampling a Nonconducting State

The TmCorA crystal structure shows a very long pore with several constrictions along the putative permeation pathway, which has been interpreted to suggest that the structure represents a ''closed'' or nonconductive conformation (Lunin et al., 2006). To complement this observation, we calculated the electrostatic potential profile across the pore using a simple solution to the Poisson-Boltzmann equation (Baker et al., 2001; Beckstein et al., 2004). The results are shown in Figure 8A and correspond to the transfer free energy of Mg^{2+} from bulk to a given position on the permeation pathway superimposed to the diameter profile (calculated using the program HOLE; Smart et al., 1996).

This energy profile shows three large barriers that are incompatible with ion permeation under physiological conditions. The energy barriers coincide with restriction points on the radius profile and correspond to position M302, L294, and M291, likely candidates to form a functional gate for Mg^{2+} permeation. Due to its hydrophobic nature, the constriction at L294 represents the highest barrier on the energy profile. Interestingly, two of these residues failed to express (M291C) or expressed at a very low yield (L294C) when compared with the rest of the mutants (Figure S2). Our calculation reveals a large overall electrostatic repulsion along the pore and argues very strongly that the conformation captured by crystallography represents indeed a nonconductive form of CorA. Moreover, the fact that the energy profile is positive along the main part of the long pore suggests that long-range conformational rearrangements would be require for Mg^{2+} translocation through this putative pathway. This is supported by our present EPR data set. First, NiEdda profile shows that the pore is not wide enough to allow NiEdda penetration. Second, EPR spectra of positions around the constrictions of the pore show strongly immobilized components (Figure S6).

The electrostatic energy profile along the pore of CorA also reveals the presence of three energy wells that would allow Mg^{2+} to bind. Two of these have been revealed in different structural data sets: Starting from the cytoplasmic entrance, the first binding site (from intracellular to extracellular side) is formed by an aspartate ring at position 277 (Eshaghi et al., 2006).

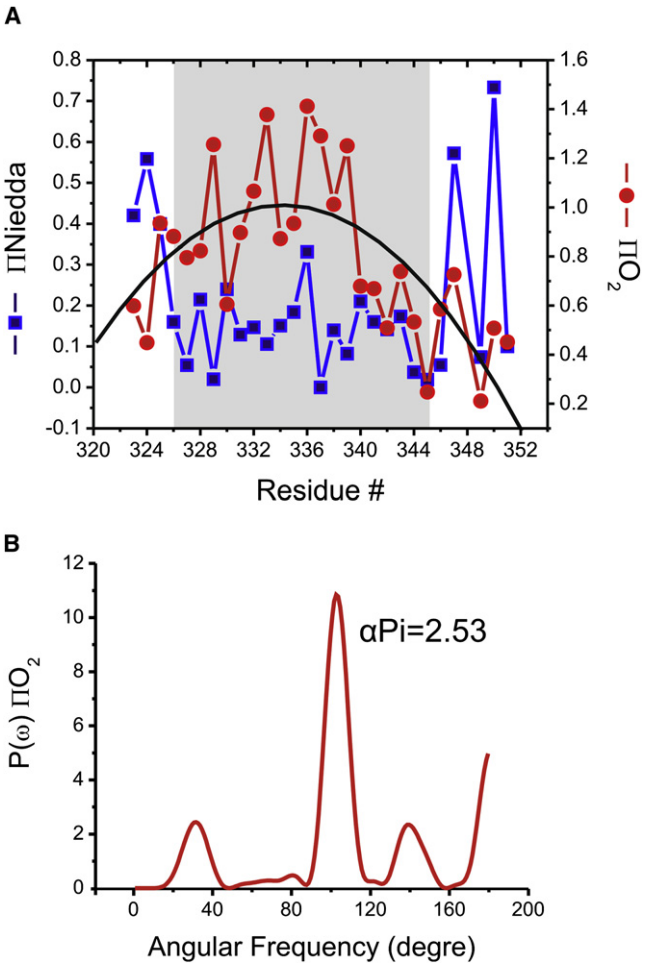

Figure 5. Membrane Footprint on TM2

(A) NiEddA and O_2 accessibility data are shown for TM2. ΠO_2 values are fitted with a parabolic function. The maximum of the function correspond to the center of the lipid bilayer. The hydrophobic core of the membrane is symbolized by the shaded gray area on the plot.

(B) Fourier transform power spectra of ΠO_2 shows a major peak around 100 degres of angular frequency consistent with the alpha helical periodicity of the whole segment. An alpha periodicity index value ≥ 2 shows that the secondary structure assignment is statistically significant.

The second one, closer to the entrance of the pore is formed by the carbonyl of the backbone of the residue G309 and G312 (Payandeh and Pai, 2006). The density observed in the latter binding site suggests the presence of a hydrated cation, although this binding site was not revealed in the highest resolution data set (Eshaghi et al., 2006). The third putative Mg^{2+} binding site suggested by our calculation corresponds to the periplasmic loop modeled in this study, which could act as a potential recognition site for divalent cation. The electrostatic surface potential of our structural model equilibrated in a dielectric slab argues for a strongly negatively charged surface centered on the conserved Glutamate 316 (Figure 8B). At this point, we can envision two roles for the periplamsic loop that are not exclusive from one to each other. Either the loop acts as a "selectivity filter" and is responsible for the primary selection of Mg^{2+} among other cation and/or it acts as an electronegative sink which increases the local concentration of cation at the external mouth of the pore.

DISCUSSION

In line with the unique biological chemistry of Mg^{2+}, CorA has no homology with any other type of transporter or membrane protein and its structure revealed an unprecedented fold and some unexpected features (Lunin et al., 2006). First, the very narrow pore is surprisingly long (>40 Å), and, unlike K^+ channels (Doyle et al., 1998), the absence of obviously coordinated Mg^{2+} ions along the putative permeation pathway limits our insights into the physical principles for Mg^{2+} permeation and selectivity.

Here, we present four strong arguments supporting the idea that Mg^{2+}-bound *Tm*CorA has a similar average conformation in a lipid bilayer as that seen in crystal structures. First, the ΠNiEdda profile shows a water-filled cavity in the large cytoplasmic funnel-like structure, anchored by a long α-helix that extends into the TM1 segment. Second, we observe very low NiEdda accessibility toward the central cavity, confirming that the long pore is mainly occluded. Third, our data also confirm the topology of the two transmembrane segments, with TM1 being mostly shielded from the membrane by TM2, which sits at the periphery and interacts directly with the lipid bilayer. Finally, all the positions where the spectra show characteristic spin-spin dipolar coupling are in close proximity in the crystal structure, pointing toward the center of the cavity. However, we do not observe spin-spin coupling in all expected positions: most sites deep in the pore along the five-fold axis of symmetry lack the expected broadening due to interspin interactions. This is reasonable if one considers the steric restriction that would allow no more than one spin probe to be attached per *Tm*CorA at the narrow regions of the permeation pathway.

The EPR accessibility data show that the footprint of the TM segments in the lipid bilayer is located between residue 325 and 345 in TM2, where at one end, four positively charged residues are likely positioned to interact with negatively charged lipid. Strikingly, our results point toward a very dynamic nature of TM2, while at the same time maintaining the expected highly periodic ΠO_2 of a stable α-helix. Given that probe dynamics is a direct reflection of backbone motion (Columbus and Hubbell, 2002), it is tempting to hypothesize that the highly dynamic behavior of TM2 could play a role in the gating/transport mechanism.

The precise role of the loop that contains the highly conserved signature sequence for the CorA family remains an open issue, since we lack both a structural template and a quantitative functional assay. This situation is also complicated by the relatively low sequence identity in the CorA family (Niegowski and Eshaghi, 2007). Recent functional studies in an eukaryotic CorA homolog from yeast have shown that the negatively charged glutamate in the loop is essential to magnesium influx (Schindl et al., 2007; Weghuber et al., 2006). Nevertheless, CorA from *Methanococcus jannaschii* and from *Mycobacterium tuberculosis,* where Mg^{2+} uptake has been characterized, does not have negatively charged residues in the loop (Hu et al., 2009; Smith et al., 1998). As in the yeast transporter, the periplasmic loop in *Tm*CorA includes two negatively charged residues,

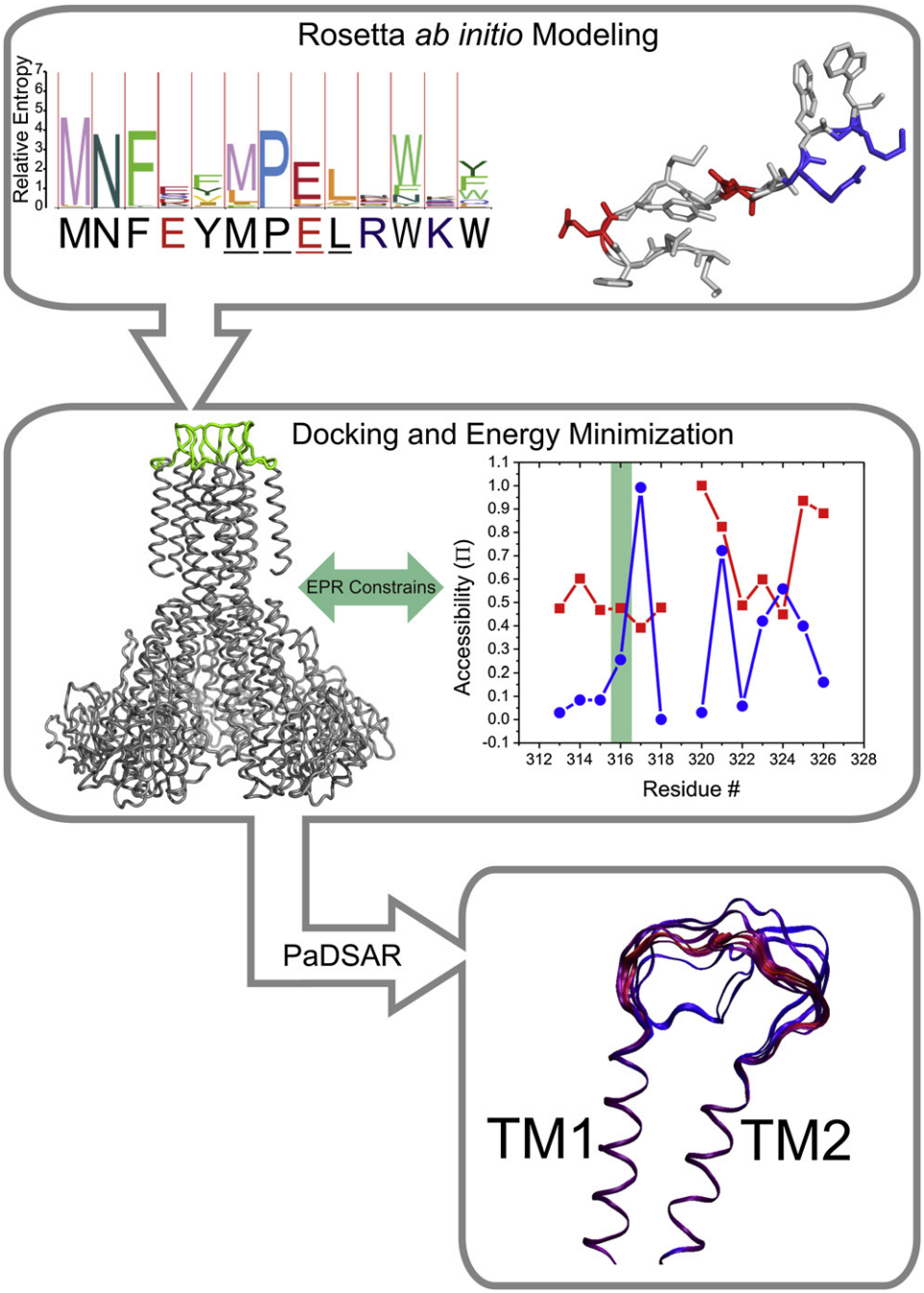

Figure 6. Modeling Strategy to Build the Structural Model of the Periplasmic Loop in CorA

The conservation of residues among the family is illustrated by the Hidden Markov model Logo profile where the height of the letter is scaled to the relative entropy of the sequence alignment. On the template generated with Rosetta, the conserved glutamate as well as the two positively charged residues are colored in red (acidic) and blue (basic). The EPR constrains used for modeling the loop are plotted in red (ΠO_2) and blue (ΠNiedda). The positions that show spin-spin coupling are highlighted in green. The bottom panel represents the evolution of the conformation of the model. The start and end points of the PaDSAR simulation are superimposed and are shown as color gradient from blue to red. After 1 ns of simulation, there is not much difference in rmsd (Figure S7), suggesting that structures fluctuate around a minimum within a RMSD of 1.3 Å. The red structure was used for all data mapping and other analysis throughout the manuscript.

E316 and E320. When neutralized, both lead to a loss of function as seen in an in vivo survival assay (Payandeh et al., 2008). Here, we propose an explicit model for the periplasmic loop, obtained in a lipid bilayer and at high [Mg^{2+}]. Our model was generated using a recently developed algorithm that parameterizes EPR-derived solvent accessibility data as structural constraints to drive a known reference structure (Sompornpisut et al., 2008). In our loop model, residue 316 converges toward the axis of

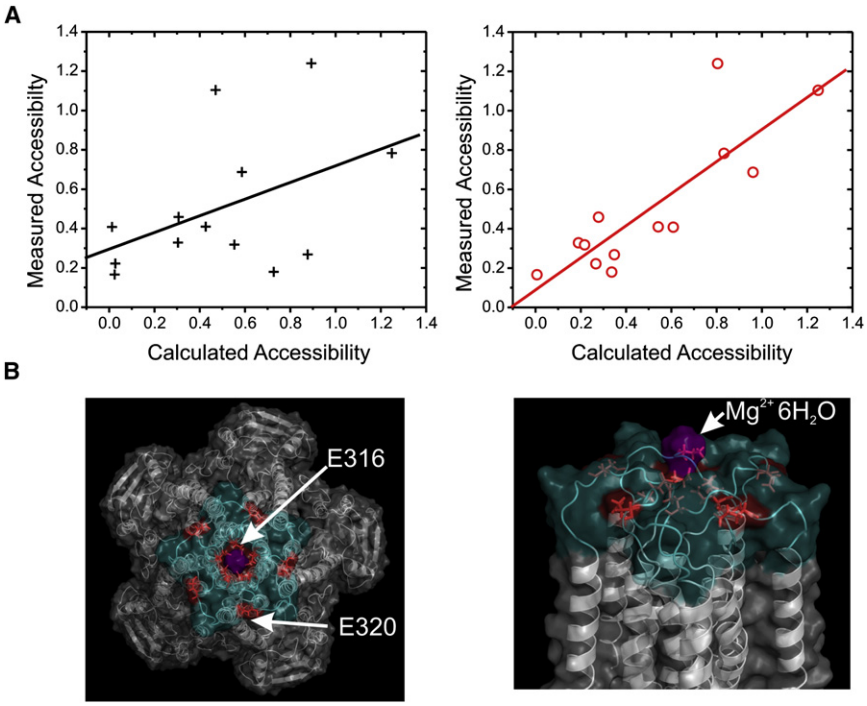

Figure 7. Evaluation of the CorA Periplasmic Loop Model

(A) Correlation plot between experimentally measured solvent accessibility and calculated accessibility for the initial model (black) and the refined structure (red).

(B) Top and side view of CorA model. The refined region is highlighted in blue. The conserved glutamate residues are colored in red. A hydrated Mg^{2+} is modeled and favorably docked at the entrance of the pore (colored in magenta).

symmetry, adopting a configuration that could in principle accommodate a hydrated Mg^{2+} (Figure 7), a feature that is consistent with the observed blocking effect of cobalt hexammine (Kucharski et al., 2000; Lunin et al., 2006). A calculated electrostatic surface potential of the loop model reveals a very strong negative isopotential surface at the mouth of the pore. This would increase the local cation concentration, favoring Mg^{2+} uptake in bacteria facing a low Mg^{2+}environment (Papp-Wallace and Maguire, 2008). The electrostatic potential along the pore is also consistent with a site that is able to accommodate Mg^{2+} and argues for a role as a primary binding site for ion recognition. However, defining the precise role of these charges in CorA will require a more robust and sensitive functional assay for CorA than the qualitative survival assay currently available.

The putative permeation path in *Tm*CorA is about 40 Å long and presents two narrow constrictions near the hydrophobic residues L294 and M291 (pore radius of 1.37 Å and 1.22 Å). These constrictions are associated with large energy barriers to the passage of ions (Figure 8A), as derived from the electrostatic energy required for the transfer of Mg^{2+} from an aqueous solution to the pore of *Tm*CorA. These constrictions represent natural candidates to regulate the flow of Mg^{2+} ions. But are these the only potential gates in CorA? The electrostatic energy profile also shows that, in addition to the obvious steric restrictions, most of the narrow transmembrane pore appears unable to accommodate a naked ion (Figure 8A). This is consistent with the idea that the conformation trapped in the crystal structures (and its equivalent membrane-embedded conformation) represents a nonconducting form of CorA and implies that long range conformational changes are required to allow Mg^{2+} permeation.

In conclusion, we have characterized the structural dynamic properties of the transmembrane elements of *Tm*CorA using site-directed spin labeling and EPR spectroscopy. Our results establish the overall structural validity of the recent crystal structures as a model for CorA in its native environment and helped generate a model for the conserved extracellular loop that contains the CorA signature sequence. This functionally important loop might serve as an electrostatic sink in the process of ion permeation and could contribute to a Mg^{2+} binding site critical for divalent selectivity.

EXPERIMENTAL PROCEDURES

Mutagenesis-Protein Expression and Purification

Cora-Pet15b vector was a generous gift from Dr. Aled Edwards. Single cysteine mutations were introduced by PCR-based mutagenesis on a Cys-Less background vector (C135S), and the entire gene was sequenced for each of them. Cystein mutants were expressed in *E. coli* BL21 DE3 PlysS strain induced by 0.5 mM IPTG at 30°C for 4 hr. Cells were harvest and disrupted using a high-pressure homogenizer (AVESTIN C-3) and the membrane were prepared by ultracentrifugation at 100,000 g for 1 hr. Membrane were solubilized at room temperature for 1 hr under gentle mixture with a solubilization buffer (50 mM HEPES/NaOH [pH 7.5], 200 mM NaCl, 10 mM $MgCl_2$, 5 mM imidazol, 10 mM DDM, and 5 mM β-mercaptoethanol). The solubilized fractions were cleared by ultracentrifugation and loaded into an immobilized cobalt affinity chromatography column (Clontech) and washed with 20 column volumes of buffer containing 0.5 mM DDM, 20 mM imidazol, and 0.5 mM TCEP (Pierce). Proteins were eluted by 250 mM imidazol containing buffer, and the hydrodynamic behavior of each mutant was assayed by analytical FPLC on a Superdex 200G 5/150 column (Amersham).

Labeling and Reconstitution

Immediately after elution from the cobalt column, the purified proteins were reacted with a 10 molar excess of spin label ([1-oxyl-2,2,5,5-tetramethylpyrrolidin-3-yl]methyl-methanethiosulfonate) for 30 min on ice, followed by second addition of 5 molar nitroxide excess and reacted for an additional 30 min. The reaction was stopped by addition of 1000-fold excess of L-cysteine and the excess probe was removed by gel filtration chromatography. High-efficiency liposome reconstitution was carried out by destabilizing the preformed liposomes with a saturating concentration of Triton X-100 (Rsat) before adding labeled protein to the liposome suspension (see Figure S3) (Knol et al., 1998). POPC-POPG 3:1 liposomes were destabilized by addition of Triton X-100 in a 0.2 w/w detergent/lipid ratio, and, after 30 min of gentle stirring, 2 mg of labeled protein was added in a 1/1500 protein/lipid molar ratio.

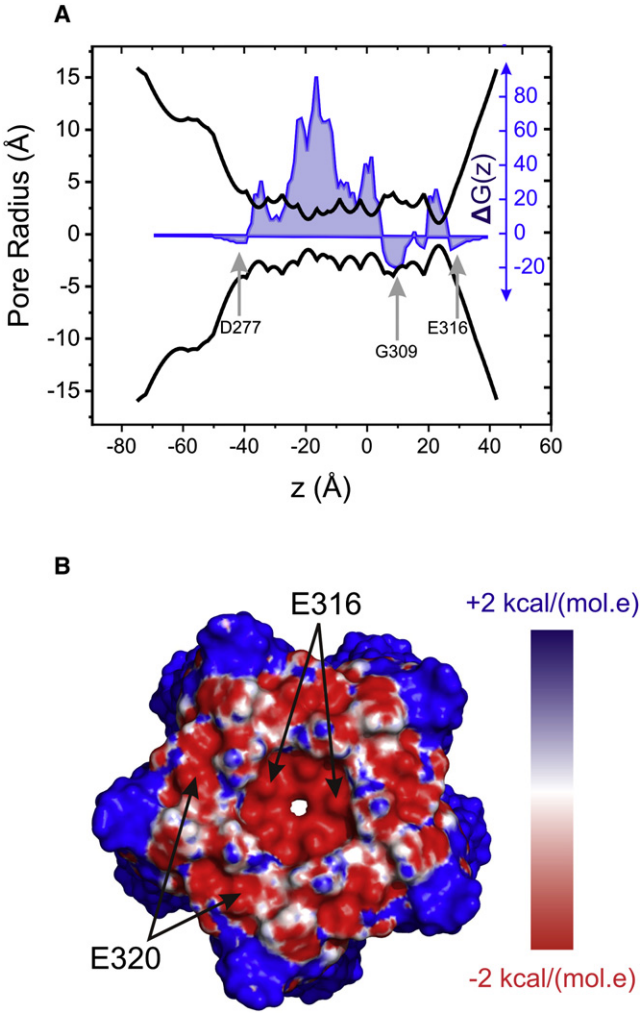

Figure 8. Electrostatic Analysis of the Refined Model

(A) The pore radius profile generated by Hole (Smart et al., 1993) plotted in black is superimposed to the electrostatic energy profile in blue.

(B) Electrostatic surface potential generated by solving the Poisson-Boltzmann equation on the refined model is scaled from −2 to +2 kcal/(mol.e) and color coded according to the spectrum at right (inset). The arrows point to glutamate 316 and glutamate 320.

Detergent was removed by successive addition (3×) of 80 mg Bio-Beads SM-2 (Bio-Rad), and proteoliposomes were harvested by ultracentrifugation at 200,000 g and resuspended into 200 μl of reconstitution buffer containing 10 mM of $MgCl_2$.

Fluorescence Measurement

Protein self-aggregation in membrane was evaluated using FRET measurements as described (Cuello et al., 2004). Mutants were labeled with a 10-fold molar excess of fluorescein-maleimide or tetramethylrhodamine-maleimide for 1 hr at room temperature (Invitrogen). Purified and labeled L12C mutant were mixed in equal proportion prior to reconstitution into various lipid vesicles at different molar ratio. Proteoliposomes were diluted below OD_{280nm} = 0.1 to avoid an overwhelming light scattering signal and fluorescence emission spectra were recorded from 505 to 700 nm on a steady-state photon counting fluorimeter (PTI-QuantaMaster40) with an excitation wavelength set at 490 nm, using slit diameter of 2 and 4 nm for excitation and emission, respectively. Lateral protein aggregation was estimated from the enhancement of the acceptor emission at 570 nm.

CW-EPR Measurement and Data Analysis

Continuous-wave EPR spectroscopic measurements were performed at room temperature on a Bruker EMX X-band spectrometer equipped with a dielectric resonator (ER 4123D). Spin-labeled samples were loaded into a gas-permeable TPX plastic capillary and spectra were recorded at 2.0 mW incident power, 100 kHz modulation frequency with 1.0 G of modulation amplitude. The motional freedom of the spin label was quantified as a peak-to-peak first-derivative width of the central resonance line (ΔH^{-1})(McHaourab et al., 1996). Solvent exposure was measured form power-saturation experiments in which the vertical peak-to-peak amplitude of the central line of the EPR spectra is measured as a function of increasing incident microwave power (Altenbach et al., 1989; Farahbakhsh et al., 1992; Perozo et al., 1998). Prior and during the recording of the spectra the sample are equilibrated with N_2, air (20% O_2), or with 25 mM NiEdda(Ni[II]ethylenediaminediacetic acid) in presence of N_2. Data were fitted to the equation:

$$f = \frac{(ax)}{\left(1 + \frac{\left(1 + (\sqrt[h]{2} - 1)\right) \times x^2}{p_{\frac{1}{2}}}\right)^h}$$

to determine the value of $P_{1/2}$ that corresponds to the incident power at which the signal is half of what it would be if no saturation occurred (Altenbach et al., 1989). The $P_{1/2}$ parameter was used to calculate the accessibility parameter Π:

$$\Pi = \frac{\Delta P_{\frac{1}{2}}(X)}{P_{\frac{1}{2}}(DPPH)} \frac{\Delta H_0(DPPH)}{\Delta H_0},$$

where DPPH (2,2-diphenyl-1-picrylhydrazyl) served as internal reference. High accessibility of the spin probe to O_2 is witness by a high value of the ΠO_2 and is diagnostic of a membrane exposed residue, whereas high NiEdda accessibility (ΠNiEdda) is diagnostic of a water exposed residue. The periodicity of a given environmental parameter was evaluated by frequency analysis in Fourier space as described previously (Cornette et al., 1987; Donnelly et al., 1994). The significance of the periodicity revealed by the power spectra is evaluated by the calculation of the α-helix periodicity index, αPI, which represents the value of P(ω) in the α-helical space relative to the total area of the entire angular space of the spectrum, and calculated as follow (Cornette et al., 1987):

$$\alpha PI = \frac{\frac{1}{40}\int_{80^\circ}^{120^\circ} p(\omega)d\omega}{\frac{1}{180}\int_{0^\circ}^{180^\circ} p(\omega)d\omega}.$$

Segments with a value of αPI ≥ 2 are considered to be α-helical. To determine the location of the solvent-accessible side of a helix, all Π values are plotted in polar coordinates and the resultant vector from the sum of all values was calculated as followed (Eisenberg et al., 1984):

$$M(\omega) = \left\{\sum_{j=1}^{N} m_j \cos(j\omega)\right\}^2 + \left\{\sum_{j=1}^{N} m_j \sin(j\omega)\right\}^2,$$

where m_j is the environmental parameter at position j along the sequence.

The EPR data were mapped into the X-ray crystal structure of CorA (code PDB 2IUB) using the program VMD (Humphrey et al., 1996). Figures were prepared with the program Pymol (DeLano, 2002) and UCSF Chimera (Pettersen et al., 2004).

Sequence Alignment and Molecular Modeling

CorA homologs were identified with the program BLAST versus a nonredundant protein database (Altschul et al., 1990), aligned with the algorithm clustalW (Thompson et al., 1994), and HMM logos were generated as previously described (Schuster-Bockler et al., 2004). Unresolved loop region of CorA is built using EPR-determined solvent accessibility restraints. Initial model is generated using ROSETTA, a computational method to predict the three-dimensional structure of a folded protein from its linear sequence of amino acids. This model is further subjected to pseudo atom approach that is developed in our laboratory, wherein the loop region is modeled using the EPR

constrains. In brief, pseudo atoms representing spin-label probes are attached to residues on the loop (313–326), and molecular dynamics simulations are carried out in which interactions between EPR probes and pseudo-atoms representing NiEdda (representing bulk solvent) and O_2 (representing hydrophobic core) are enforced to mimic the experimental data. The resulting model is arranged as five-fold symmetric structure with resolved loop region.

Electrostatic Energy Profile Calculation and Pore Radius Determination

The transfer free energy of a divalent magnesium ion from bulk to a position on the permeation pathway is calculated using Poisson-Boltzmann equation. The large barrier for Mg^{2+} permeation in the crystal state comes from the high reaction field energy along the pore in the transmembrane region. A high reaction field is a consequence of the narrow permeation path.

The electrostatic surface potential of our EPR-constrained model was generated by solving the Poisson Boltzmann equation using PBEQ solver as previously described (Jo et al., 2008). The system was equilibrated in a dielectric slab mimicking the membrane environment (dielectric constant = 2) at pH = 7 in presence of 300 mM of ions. The result were scaled and mapped using Pymol (DeLano, 2002).

SUPPLEMENTAL INFORMATION

Supplemental Information includes eight figures and can be found with this article online at doi:10.1016/j.str.2010.04.009.

ACKNOWLEDGMENTS

This work was supported by NIH grant # R01 GM088406. O.D. received a postdoctoral fellowship from fondation pour la recherche médicale. We are thankful to Francisco Bezanilla for sharing access to his fluorimeter and to Jose S. Santos for helpful comments and advice with manuscript preparation. O.D. and E.P designed the research; O.D., L.G.C., V.J., and D.M.C performed the research; B.R. contributed to a new analytic tool; O.D., L.G.C., and E.P. analyzed data; and O.D. and E.P. wrote the manuscript.

Received: December 17, 2009
Revised: April 3, 2010
Accepted: April 7, 2010
Published: July 13, 2010

REFERENCES

Altenbach, C., Froncisz, W., Hyde, J.S., and Hubbell, W.L. (1989). Conformation of spin-labeled melittin at membrane surfaces investigated by pulse saturation recovery and continuous wave power saturation electron paramagnetic resonance. Biophys. J. *56*, 1183–1191.

Altenbach, C., Greenhalgh, D.A., Khorana, H.G., and Hubbell, W.L. (1994). A collision gradient method to determine the immersion depth of nitroxides in lipid bilayers: application to spin-labeled mutants of bacteriorhodopsin. Proc. Natl. Acad. Sci. USA *91*, 1667–1671.

Altschul, S.F., Gish, W., Miller, W., Myers, E.W., and Lipman, D.J. (1990). Basic local alignment search tool. J. Mol. Biol. *215*, 403–410.

Baker, N.A., Sept, D., Joseph, S., Holst, M.J., and McCammon, J.A. (2001). Electrostatics of nanosystems: application to microtubules and the ribosome. Proc. Natl. Acad. Sci. USA *98*, 10037–10041.

Beckstein, O., Tai, K., and Sansom, M.S. (2004). Not ions alone: barriers to ion permeation in nanopores and channels. J. Am. Chem. Soc. *126*, 14694–14695.

Bonneau, R., Strauss, C.E., Rohl, C.A., Chivian, D., Bradley, P., Malmstrom, L., Robertson, T., and Baker, D. (2002). De novo prediction of three-dimensional structures for major protein families. J. Mol. Biol. *322*, 65–78.

Columbus, L., and Hubbell, W.L. (2002). A new spin on protein dynamics. Trends Biochem. Sci. *27*, 288–295.

Cornette, J.L., Cease, K.B., Margalit, H., Spouge, J.L., Berzofsky, J.A., and DeLisi, C. (1987). Hydrophobicity scales and computational techniques for detecting amphipathic structures in proteins. J. Mol. Biol. *195*, 659–685.

Cuello, L.G., Cortes, D.M., and Perozo, E. (2004). Molecular architecture of the KvAP voltage-dependent K+ channel in a lipid bilayer. Science *306*, 491–495.

Dalmas, O. (2007). Magnesium selective ion channels. Biophys. J. *93*, 3729–3730.

DeLano, W.L. (2002). The Pymol Molecular Graphics System (Palto Alto, CA: DeLano Scientific).

Donnelly, D., Overington, J.P., and Blundell, T.L. (1994). The prediction and orientation of alpha-helices from sequence alignments: the combined use of environment-dependent substitution tables, Fourier transform methods and helix capping rules. Protein Eng. *7*, 645–653.

Doyle, D.A., Morais Cabral, J., Pfuetzner, R.A., Kuo, A., Gulbis, J.M., Cohen, S.L., Chait, B.T., and MacKinnon, R. (1998). The structure of the potassium channel: molecular basis of K+ conduction and selectivity. Science *280*, 69–77.

Eisenberg, D., Weiss, R.M., and Terwilliger, T.C. (1984). The hydrophobic moment detects periodicity in protein hydrophobicity. Proc. Natl. Acad. Sci. USA *81*, 140–144.

Eshaghi, S., Niegowski, D., Kohl, A., Martinez Molina, D., Lesley, S.A., and Nordlund, P. (2006). Crystal structure of a divalent metal ion transporter CorA at 2.9 angstrom resolution. Science *313*, 354–357.

Farahbakhsh, Z.T., Altenbach, C., and Hubbell, W.L. (1992). Spin labeled cysteines as sensors for protein-lipid interaction and conformation in rhodopsin. Photochem. Photobiol. *56*, 1019–1033.

Gouaux, E., and Mackinnon, R. (2005). Principles of selective ion transport in channels and pumps. Science *310*, 1461–1465.

Hmiel, S.P., Snavely, M.D., Miller, C.G., and Maguire, M.E. (1986). Magnesium transport in Salmonella typhimurium: characterization of magnesium influx and cloning of a transport gene. J. Bacteriol. *168*, 1444–1450.

Hmiel, S.P., Snavely, M.D., Florer, J.B., Maguire, M.E., and Miller, C.G. (1989). Magnesium transport in Salmonella typhimurium: genetic characterization and cloning of three magnesium transport loci. J. Bacteriol. *171*, 4742–4751.

Hu, J., Sharma, M., Qin, H., Gao, F.P., and Cross, T.A. (2009). Ligand binding in the conserved interhelical loop of CorA, a magnesium transporter from Mycobacterium tuberculosis. J. Biol. Chem. *284*, 15619–15628.

Humphrey, W., Dalke, A., and Schulten, K. (1996). VMD: visual molecular dynamics. J. Mol. Graph. *14*, 33–38, 27–28.

Jo, S., Vargyas, M., Vasko-Szedlar, J., Roux, B., and Im, W. (2008). PBEQ-Solver for online visualization of electrostatic potential of biomolecules. Nucleic Acids Res. *36*, W270–W275. 10.1093/nar/gkn314.

Kehres, D.G., Lawyer, C.H., and Maguire, M.E. (1998). The CorA magnesium transporter gene family. Microb. Comp. Genomics *3*, 151–169.

Killian, J.A., and von Heijne, G. (2000). How proteins adapt to a membrane-water interface. Trends Biochem. Sci. *25*, 429–434.

Knol, J., Sjollema, K., and Poolman, B. (1998). Detergent-mediated reconstitution of membrane proteins. Biochemistry *37*, 16410–16415.

Kucharski, L.M., Lubbe, W.J., and Maguire, M.E. (2000). Cation hexaammines are selective and potent inhibitors of the CorA magnesium transport system. J. Biol. Chem. *275*, 16767–16773.

Lunin, V.V., Dobrovetsky, E., Khutoreskaya, G., Zhang, R., Joachimiak, A., Doyle, D.A., Bochkarev, A., Maguire, M.E., Edwards, A.M., and Koth, C.M. (2006). Crystal structure of the CorA Mg2+ transporter. Nature *440*, 833–837.

Maguire, M.E. (1992). MgtA and MgtB: prokaryotic P-type ATPases that mediate Mg2+ influx. J. Bioenerg. Biomembr. *24*, 319–328.

McHaourab, H.S., Lietzow, M.A., Hideg, K., and Hubbell, W.L. (1996). Motion of spin-labeled side chains in T4 lysozyme. Correlation with protein structure and dynamics. Biochemistry *35*, 7692–7704.

Niegowski, D., and Eshaghi, S. (2007). The CorA family: structure and function revisited. Cell. Mol. Life Sci. *64*, 2564–2574.

Papp-Wallace, K.M., and Maguire, M.E. (2008). Regulation of CorA Mg2+ channel function affects the virulence of Salmonella enterica serovar typhimurium. J. Bacteriol. *190*, 6509–6516.

Payandeh, J., and Pai, E.F. (2006). A structural basis for Mg2+ homeostasis and the CorA translocation cycle. EMBO J. *25*, 3762–3773.

Payandeh, J., Li, C., Ramjeesingh, M., Poduch, E., Bear, C.E., and Pai, E.F. (2008). Probing structure-function relationships and gating mechanisms in the CorA Mg2+ transport system. J. Biol. Chem. *283*, 11721–11733.

Perozo, E., Cortes, D.M., and Cuello, L.G. (1998). Three-dimensional architecture and gating mechanism of a K+ channel studied by EPR spectroscopy. Nat. Struct. Biol. *5*, 459–469.

Perozo, E., Cortes, D.M., and Cuello, L.G. (1999). Structural rearrangements underlying K+-channel activation gating. Science *285*, 73–78.

Perozo, E., Cuello, L.G., Cortes, D.M., Liu, Y.S., and Sompornpisut, P. (2002). EPR approaches to ion channel structure and function. Novartis Found. Symp. *245*, 146–158, discussion, 158–164, 165–148.

Pettersen, E.F., Goddard, T.D., Huang, C.C., Couch, G.S., Greenblatt, D.M., Meng, E.C., and Ferrin, T.E. (2004). UCSF Chimera—a visualization system for exploratory research and analysis. J. Comput. Chem. *25*, 1605–1612.

Rohl, C.A., Strauss, C.E., Chivian, D., and Baker, D. (2004). Modeling structurally variable regions in homologous proteins with rosetta. Proteins *55*, 656–677.

Schindl, R., Weghuber, J., Romanin, C., and Schweyen, R.J. (2007). Mrs2p forms a high conductance Mg2+ selective channel in mitochondria. Biophys. J. *93*, 3872–3883.

Schueler-Furman, O., Wang, C., Bradley, P., Misura, K., and Baker, D. (2005). Progress in modeling of protein structures and interactions. Science *310*, 638–642.

Schuster-Bockler, B., Schultz, J., and Rahmann, S. (2004). HMM Logos for visualization of protein families. BMC Bioinformatics *5*, 7.

Smart, O.S., Goodfellow, J.M., and Wallace, B.A. (1993). The pore dimensions of gramicidin A. Biophys. J. *65*, 2455–2460.

Smart, O.S., Neduvelil, J.G., Wang, X., Wallace, B.A., and Sansom, M.S. (1996). HOLE: a program for the analysis of the pore dimensions of ion channel structural models. J. Mol. Graph. *14*, 354, 360, 376.

Smith, R.L., Gottlieb, E., Kucharski, L.M., and Maguire, M.E. (1998). Functional similarity between archaeal and bacterial CorA magnesium transporters. J. Bacteriol. *180*, 2788–2791.

Sompornpisut, P., Roux, B., and Perozo, E. (2008). Structural refinement of membrane proteins by restrained molecular dynamics and solvent accessibility data. Biophys. J. *95*, 5349–5361.

Thompson, J.D., Higgins, D.G., and Gibson, T.J. (1994). CLUSTAL W: improving the sensitivity of progressive multiple sequence alignment through sequence weighting, position-specific gap penalties and weight matrix choice. Nucleic Acids Res. *22*, 4673–4680.

Vasquez, V., Sotomayor, M., Cortes, D.M., Roux, B., Schulten, K., and Perozo, E. (2008). Three-dimensional architecture of membrane-embedded MscS in the closed conformation. J. Mol. Biol. *378*, 55–70.

Weghuber, J., Dieterich, F., Froschauer, E.M., Svidova, S., and Schweyen, R.J. (2006). Mutational analysis of functional domains in Mrs2p, the mitochondrial Mg2+ channel protein of Saccharomyces cerevisiae. FEBS J. *273*, 1198–1209.

 ©2010 Elsevier Ltd All rights reserved